Materials Science and Technology

ISSN: 0267-0836 (Print) 1743-2847 (Online) Journal homepage: http://www.tandfonline.com/loi/ymst20

Wear resistance of Fe-based amorphous coatings prepared by AC-HVAF and HVOF

H. R. Ma, J. W. Li, J. Jiao, C. T. Chang, G. Wang, J. Shen, X. M. Wang & R. W. Li

To cite this article: H. R. Ma, J. W. Li, J. Jiao, C. T. Chang, G. Wang, J. Shen, X. M. Wang & R. W. Li (2016): Wear resistance of Fe-based amorphous coatings prepared by AC-HVAF and HVOF, Materials Science and Technology

To link to this article: http://dx.doi.org/10.1080/02670836.2016.1160195

Published online: 17 Mar 2016.

Wear resistance of Fe-based amorphous coatings prepared by AC-HVAF and HVOF

H. R. Ma[1,2,3], J. W. Li[2,3], J. Jiao[4], C. T. Chang*[2,3], G. Wang*[1], J. Shen[4], X. M. Wang[2,3] and R. W. Li[2,3]

$Fe_{63}Cr_8Mo_{3.5}Ni_5P_{10}B_4C_4Si_{2.5}$ amorphous coatings have been prepared by the activated combustion high velocity air fuel (AC-HVAF) and high velocity oxygen fuel (HVOF) processes. The microstructure and wear resistance of the amorphous coatings are comparatively studied. The wear volume loss of the AC-HVAF coating is approximately seven times less than that of the HVOF coating, indicating that the AC-HVAF coating exhibits better wear resistance. Detailed analysis on the worn surface indicates that the enhanced wear resistance of the AC-HVAF coating is mainly attributed to the formation of a more stable oxide tribolayer and smoother worn surface, which result from the dense and complete amorphous microstructure of the AC-HVAF coating. The wear mechanism of the amorphous coatings is dominated by oxidation wear.

Keywords: Amorphous alloys, Wear resistance, Tribological properties, Coatings, Thermal spraying

Introduction

Fe-based amorphous alloys are generally known for their unique combination of relatively low cost, high strength and hardness, outstanding corrosion and wear resistance, and good magnetic properties.[1–4] Unfortunately, these materials find limited application in the industrial field because of the limited product size, poor plastic deformation after yielding and no work hardening at room temperature.[5–7] As an alternative form of Fe-based amorphous alloys, Fe-based amorphous coatings fabricated using the thermal spraying methods can not only mitigate the drawbacks of these alloys, also maintain the excellent corrosion and wear resistance, and therefore have attracted much attention.[8–12]

Among various thermal spraying techniques, high velocity oxygen fuel (HVOF) process is known for the high kinetic energy process and relatively low flame temperature, which favours the formation of an amorphous structure with decreased porosity and oxide content.[8–10] Recently, the activated combustion high velocity air fuel (AC-HVAF) technique, using compressed air instead of pure oxygen as the combustion-supporting media for spraying, has been developed as a relatively new thermal spraying technique. The AC-HVAF shows better spraying rate and deposition efficiency in contrast with the HVOF, resulting in the as-deposited coatings with lower porosity and higher bonding strength to the substrates.[11–14] Some studies have shown that Fe-based amorphous coatings explored by AC-HVAF possess better corrosion resistance than those fabricated by HVOF.[11,12] However, there remains a lack of a detailed comparative evaluation on the wear resistance of Fe-based amorphous coatings prepared by AC-HVAF and HVOF.

In our previous work, we found that the corrosion and wear resistance of the $Fe_{63}Cr_8Mo_{3.5}Ni_5P_{10}B_4C_4Si_{2.5}$ (at.-%) amorphous coating prepared by HVOF compare favourably with those of SAM2X5 ($Fe_{49.7}Cr_{17.7}Mn_{1.9}Mo_{7.4}W_{1.6}B_{15.2}C_{3.8}Si_{2.4}$) and SAM1651 ($Fe_{48}Mo_{14}Cr_{15}Y_2C_{15}B_6$) amorphous coatings, despite the absence of W, and low Cr and Mo content.[15] In this paper, the microstructure and wear resistance of the $Fe_{63}Cr_8Mo_{3.5}Ni_5P_{10}B_4C_4Si_{2.5}$ amorphous coating prepared by both AC-HVAF and HVOF are comparatively studied. The present work shows that the wear resistance of the AC-HVAF coating is superior to that of the HVOF coating under dry sliding conditions. The wear mechanism will be correlated with the structure and composition of the worn surface.

Experimental procedures

$Fe_{63}Cr_8Mo_{3.5}Ni_5P_{10}B_4C_4Si_{2.5}$ (at.-%) powders were manufactured by high pressure Ar gas atomisation method using industrial raw materials. Powders with sizes in the range of 20–45 μm were sieved out for spraying in the present work and dried at 100°C in an oven for 1 hour to remove all residual moisture before spraying. The mild steel was selected as substrate with a dimension of 20 mm × 20 mm × 3 mm. All substrates were polished and degreased by ethanol, dried in air, and then grit-blasted prior to thermal spraying. The amorphous coatings

[1]Laboratory for Microstructures, Shanghai University, Shanghai 200444, China
[2]Key Laboratory of Magnetic Materials and Devices, Ningbo Institute of Materials Technology & Engineering, Chinese Academy of Sciences, Ningbo, Zhejiang 315201, China
[3]Zhejiang Province Key Laboratory of Magnetic Materials and Application Technology, Ningbo Institute of Materials Technology & Engineering, Chinese Academy of Sciences, Ningbo, Zhejiang 315201, China
[4]School of Materials Science and Engineering, Tongji University, 4800 Caoan Road, Shanghai 201084, China

*Corresponding authors, email ctchang@nimte.ac.cn (C. T. Chang); g.wang@shu.edu.cn (G. Wang)

Published by Taylor & Francis on behalf of the Institute
Received 13 January 2016; accepted 25 February 2016
DOI 10.1080/02670836.2016.1160195

Table 1 Spraying parameters employed in the HVOF and AC-HVAF processes

Parameters	Condition
HVOF	
Propane flow (L min^{-1})	35
Oxygen flow (L min^{-1})	25
Feed rate (g min^{-1})	50
Spraying distance (mm)	300
AC-HVAF	
Compressed air (MPa)	0.5
Propane pressure (MPa)	3.4
Airpressure (MPa)	58.3
Powder feed rate (g min^{-1})	30
Spraying distance (mm)	180

were fabricated by AC-HVAF and HVOF thermal spray systems in the open air. The detailed spraying parameters were presented in Table 1.

Field emission scanning electron microscopy (SEM, FEI Quanta FEG 250) was used to characterise the microstructure of the powders and as-sprayed coatings. Their phase structures were analysed with X-ray diffraction using Cu $K\alpha$ radiation (XRD, D8 Advance). The percentage porosity of the coatings was evaluated with the image analysis on optical microscopy (Zeiss LSM 700) and Image Pro-Plus 6.0 software.

Dry sliding friction and wear tests were performed with a reciprocating ball-on-plate tribometer (UMT-3, Center for Tribology) at ambient conditions using commercially available Al_2O_3 balls (manufacturer's nominal hardness: 16.5 GPa; diameter: 9 mm) as the counterparts. Before the wear tests, all samples were polished to mirror finish in order to obtain identical surface roughness. A sliding stroke of 7 mm, sliding speeds of 0.02 and 0.1 m s^{-1}, applied load of 20 N, and overall sliding distance of 250 m were applied in the experiments and the friction coefficient was continuously recorded during the test. New balls were used for each test. The wear volume loss was calculated using the equation of $V = S \times d$ where V is the wear volume (mm^3), S is the cross-sectional area (mm^2) of the worn surface, d means the overall sliding distance (mm), respectively. The worn surface profile was scanned by a surface profilometer (Alpha-Step IQ) and the area of the scanned profile was calculated by the Origin 8 software. Each area value is the average of four measurements conducted in the different positions of the wear track. The wear tracks were investigated by SEM coupled with energy dispersive X-ray spectroscopy (EDX, OXFORD X-Max). Furthermore, the oxide species on the wear tracks were examined by Raman spectroscopy (Renishaw inVia Reflex) using an excitation wavelength of 532 nm. For comparison, the mild steel was also selected to perform the test in the same way. Hardness measurements were measured on the surfaces of the coating and the mild steel using a Vickers hardness tester with an applied load of 9.8 N and a loading time of 15 seconds.

Results and discussion

Microstructure characterisations of the amorphous coatings

The SEM image of the feedstock powders is shown in Fig. 1*a*. It is clearly seen that the majority of powders show good sphericity and a smooth surface with diameters of 20–45 μm which are beneficial for powder flowability and spraying processes. Figure 1*b* shows the XRD patterns of the powders and the coatings prepared by HVOF and AC-HVAF, respectively. Both the powders and AC-HVAF coating show a broad halo without any distinguished sharp diffraction peaks, indicating the completely amorphous structure within the resolution limit of XRD. However, the HVOF coating exhibits an almost fully amorphous structure combined with a very tiny amount of crystalline phases of $Fe_{1.91}C_{0.09}$ and a-Fe, which should be related to the higher flame temperature and the use of pure oxygen in the HVOF process.[11,12] The cross-sectional microstructures of the as-sprayed coatings are displayed in Fig. 1*c* and *d*. The coatings prepared by HVOF and AC-HVAF have a similar thickness of 200–300 μm and adhere well to the substrates. It can be seen that there are some dark inclusions distributed at the interface between the HVAF coating and substrate. The EDS analysis (not shown here) reveals that these dark inclusions are residual Al_2O_3 grit-blasted particles. Some heterogeneous phases such as the unmelted particle and intersplat regions can be clearly observed in the HVOF coating, whereas these phases are unable to be detected in the AC-HVAF coating. The porosities of the coatings prepared by HVOF and AC-HVAF are 1.5 and 0.4%, respectively, indicating that the AC-HVAF coating has a denser microstructure than the HVOF coating.

Wear characteristics of the coatings

Figure 2*a* shows the variations of friction coefficients during dry sliding of the mild steel and amorphous coatings prepared by HVOF and AC-HVAF. The inset in Fig. 2*a* is the schematic illustration of the wear test. The amorphous coatings can keep relatively steady state wear throughout the sliding test, but the wear process of the mild steel is very unstable and accompanied by numerous waves in the curve. The result suggests that the amorphous coatings can keep slower wear loss for even much longer service time. Furthermore, the friction coefficient of the HVOF coating exhibits slight fluctuations, whereas the AC-HVAF coating shows a more stable state in the sliding process.

The average wear volume loss after completion of sliding (applied load of 20 N, sliding speed of 0.1 m s^{-1}) and the Vickers hardness of the test samples are showed in Fig. 2*b*. Both amorphous coatings show much lower wear volume loss than the mild steel, indicative of excellent wear resistant of the amorphous coatings. However, it can be seen that the wear volume of the AC-HVAF coating is approximately seven times less than that of the HVOF coating, suggesting that the AC-HVAF coating exhibits more superior wear resistance. The Vickers hardness values of the coatings are around 960 HV which are significantly higher than that of the mild steel. As is well-known, there is an inverse relationship between surface hardness and wear loss when the surfaces come into contact with each other causing friction and wear.[16,17] Therefore, the enhanced surface hardness of the amorphous coatings should be one of the reasons for superior wear resistance to that of the mild steel.

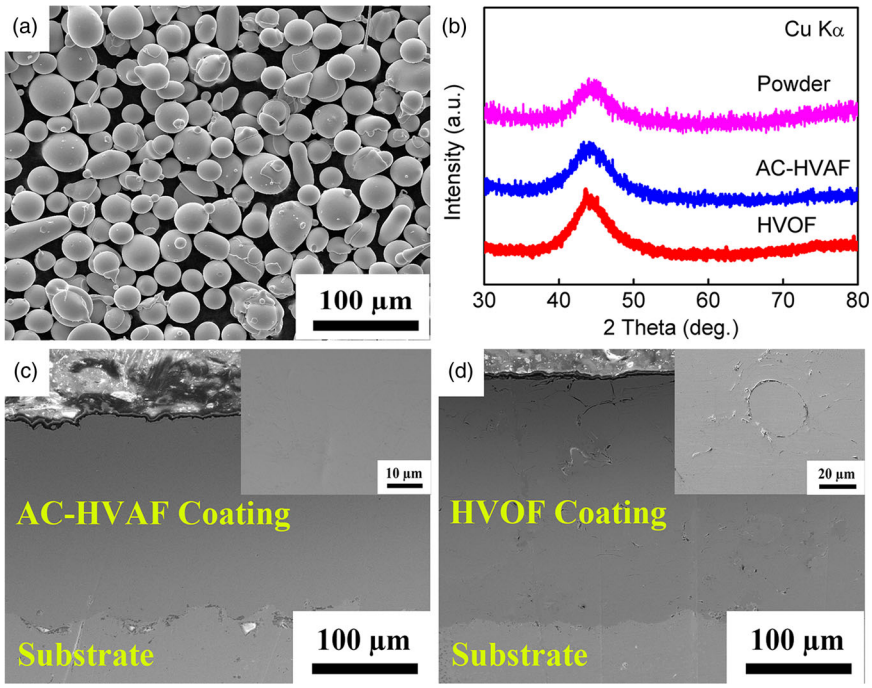

1 ***a*** **SEM micrograph of the feedstock $Fe_{63}Cr_8Mo_{3.5}Ni_5P_{10}B_4C_4Si_{2.5}$ powders obtained by gas atomisation; *b* XRD patterns of the feedstock powders and coatings prepared by AC-HVAF and HVOF; *c* and *d* SEM micrographs of the AC-HVAF and HVOF coatings. The inserts are the magnified image**

Wear mechanisms of the amorphous coatings

To understand the wear mechanism, wear tracks of the AC-HVAF and HVOF amorphous coatings after sliding at speeds of 0.02 and 0.1 m s^{-1} are shown in Fig. 3. The wear track of the AC-HVAF coating at low sliding speed, shown in Fig. 3*a*, presents a smooth worn surface with little wear, on which there are just some white or brunet island regions with small size distributed dispersedly. In the case of fast sliding speed (Fig. 3*b*), the wear track of the AC-HVAF coating contains some small pits and shallow detached areas, demonstrating more wear losses as the sliding speed increases. However, a large amount of wide and deep wear pits can be found on the wear tracks of the HVOF coatings (Fig. 3*c* and *d*), which are much wider in dimension than those of AC-HVAF coatings. This result reveals that the wear failure of the HVOF coating is much more serious. EDX analysis on the smooth part of wear tracks (sections A, B, C and D) show the existence of oxygen, implying that a smooth oxide tribolayer might form on the surface of the coating during the dry sliding process. Moreover, the content of oxygen at fast sliding speed has a dramatically increase compared to the wear track at low sliding speed. Some studies have shown that the main wear mechanism of the amorphous coating under dry frictional wear condition is oxidation wear because the high-frequency friction can apparently increase the surface temperature.[18–20] In addition, higher content of oxygen is observed on the smooth part of the wear tracks of the HVOF coating compared to the AC-HVAF coating, which will be further discussed below.

Figure 4*a* shows the SEM micrograph of an island region on the wear track of the AC-HVAF coating at speed of 0.02 m s^{-1}. The EDS results for sections E–M marked in Fig. 4 are summarised in Table 2. The smooth zone (section E) near by the island has similar oxygen content compared to that of smooth part of the wear track (section B). However, the oxygen content of the island region (section F) dramatically increases to 73.41 at.-%, which is much higher than that of the surrounding

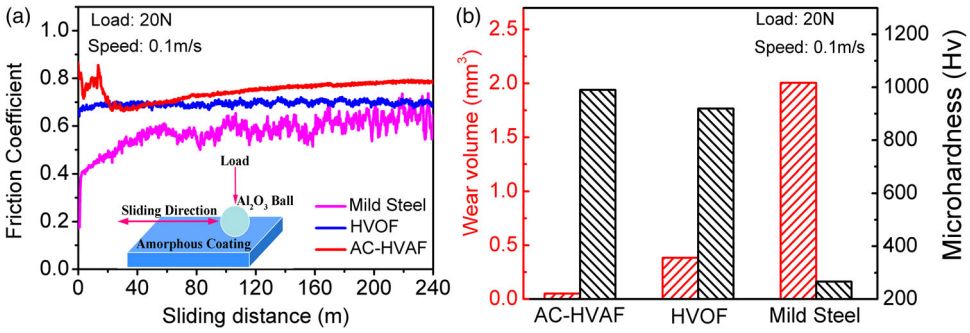

2 **Friction coefficients curves *a* and wear volume loss and Vickers hardness *b* of the mild steel and the coatings prepared by AC-HVAF and HVOF**

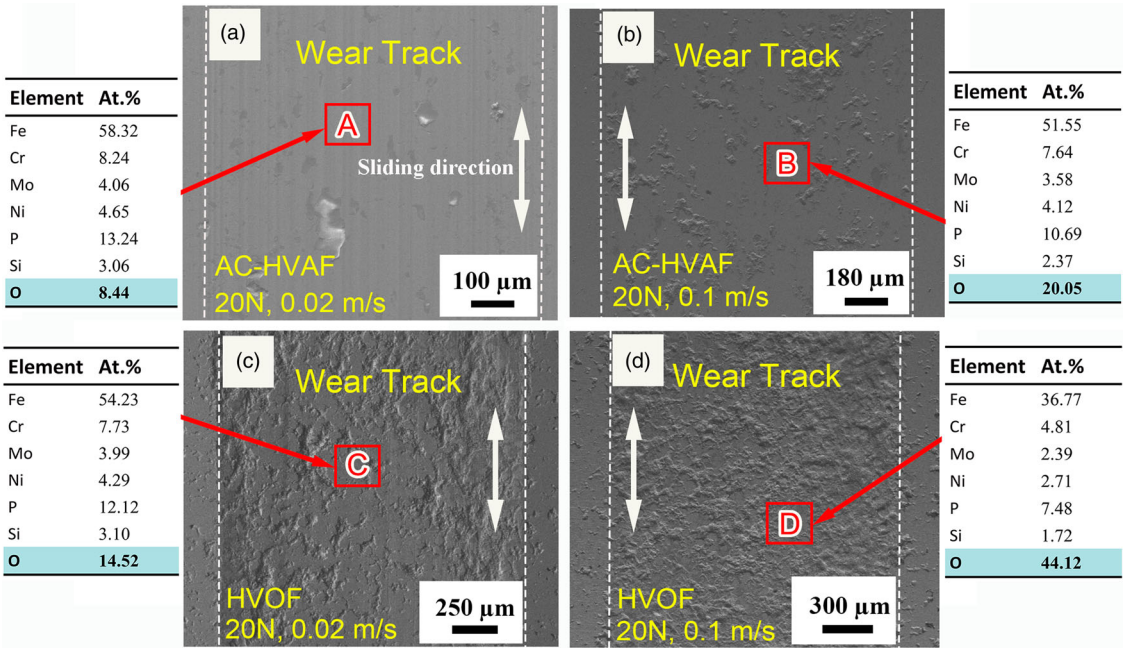

Element	At.%
Fe	58.32
Cr	8.24
Mo	4.06
Ni	4.65
P	13.24
Si	3.06
O	8.44

Element	At.%
Fe	51.55
Cr	7.64
Mo	3.58
Ni	4.12
P	10.69
Si	2.37
O	20.05

Element	At.%
Fe	54.23
Cr	7.73
Mo	3.99
Ni	4.29
P	12.12
Si	3.10
O	14.52

Element	At.%
Fe	36.77
Cr	4.81
Mo	2.39
Ni	2.71
P	7.48
Si	1.72
O	44.12

3 SEM images of wear tracks of the amorphous coatings: *a* and *b* AC-HVAF coatings at speed of 0.02 and 0.1 m s^{-1} respectively; *c* and *d* HVOF coatings at speeds of 0.02 and 0.1 m s^{-1} respectively

areas. Thus it could be proposed that the oxidation of some local regions is very serious, while most regions of the coating surface have relatively homogeneous oxidation during the friction process. It is known that the elevated average temperature of the frictional surface is limited, but the flash temperature could become very high and even exceed the melting point of alloy, resulting in much more serious oxidation.[18] Therefore, the high flash temperature should be responsible for highly oxidation of some local regions, which are usually brittle and prone to flaking off. Figure 4*b* shows the SEM image of a wear pit on the wear track of the AC-HVAF coating at high sliding speed. The same phenomenon can be also found in sections G and H, corresponding to the highly oxidised local regions and slightly oxidised smooth regions, respectively. Thus, it could be concluded that wear pits on the wear track of the AC-HVAF coating should arise from peeling off of the local highly oxidised layer.

Figure 5 shows the Raman spectrum analysis of different positions on the wear tracks of the amorphous coatings. The Raman spectra of smooth part on the wear

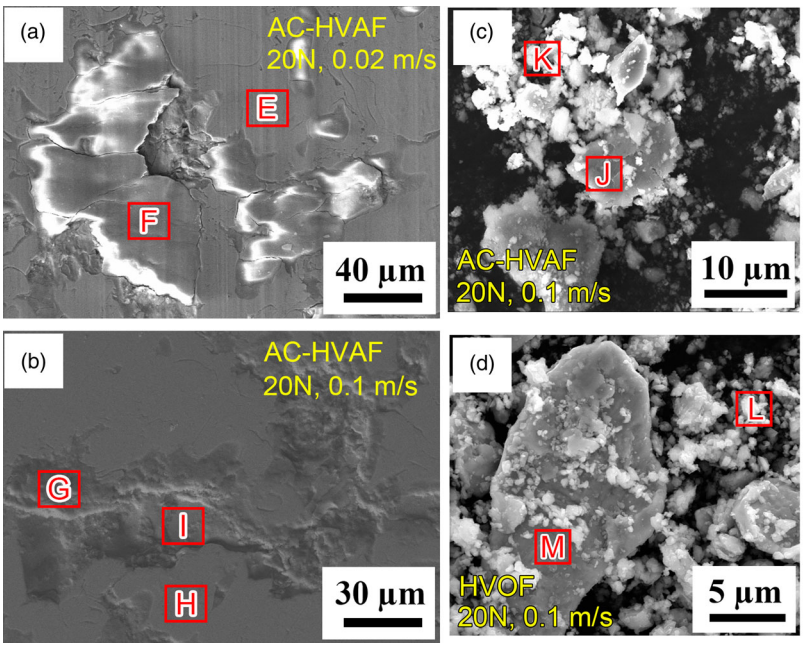

4 SEM micrographs of *a* an island region on the wear track of the AC-HVAF coating at speed of 0.02 m s^{-1}, *b* a wear pit on the wear track of the AC-HVAF coating at speed of 0.1 m s^{-1}, *c* worn-off debris of the AC-HVAF coating at speed of 0.1 m s^{-1} and *d* worn-off debris of the HVOF coating at speed of 0.1 m s^{-1}

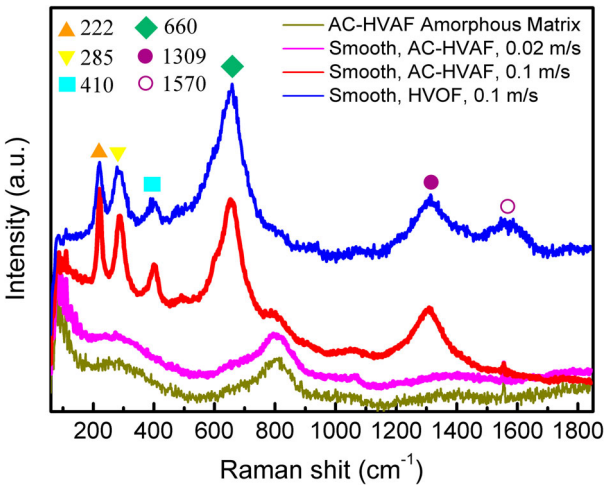

5 Raman spectrum analysis of different positions on the wear tracks of the amorphous coatings prepared by AC-HVAF and HVOF

track of the AC-HVAF coating at low sliding speed is basically the same as that of the AC-HVAF amorphous coating matrix with a broad characteristic band at near 800 cm^{-1} which should be contributed from the amorphous structure, suggesting that the slightly oxidised tribolayer keeps nearly complete amorphous structure. But the smooth part shows a surface hardness of approximately 1040 HV, which is higher than that of the coating matrix (960 HV). It is known that the NiP alloy has been widely used in the mechanical and electronic industries due to their high hardness and excellent wear resistance.[21–23] Besides, Ni-rich phases in the intersplat regions of coatings can serve as a barrier to oxygen diffusion during friction, resulting in the improvement of wear resistance.[24] It can be found that the Ni and P content in the smooth parts of the coatings are always relatively high (sections A–C). Thereby, one of the reasons for surface hardening might be the precipitation of some NiP phases in the oxidised tribolayer.[22] Oxidation process of the coating surface seriously deteriorates with increasing the sliding speed, resulting in different crystalline phases precipitating in the amorphous matrix with sharp characteristic peaks appearing in the Raman spectrum. It is seen from Fig. 5 that the wear tracks have the characteristic band contributed from Fe_3O_4 near at 222, 285, 410, 1309 cm^{-1} and the contribution of Fe_2O_3 near at 660 cm^{-1}.[22] A weak peak at near 800 cm^{-1} can still be observed in the Raman spectrum of worn surface of the AC-HVAF coating at high speed, indicating the worn surface at high speed still keeps partially amorphous structure, however, the characteristic peaks of crystalline phases are more stronger which cover up the signal of the former. The hardness of the smooth part on the wear track of the AC-HVAF coating at high sliding speed (870 HV) is lower than that at low sliding speed (1040 HV). Eventually, highly oxidised tribolayer would be brittle and flake off from the surface, as shown and described above.

Based on the above analysis, it can be summarised that the formation of a oxide layer could be a significant factor in reducing the wear loss because it acts as a protective layer.[25] The slightly oxidised tribolayer has higher hardness than the coating matrix, which can strengthen the dense structure of the coating. On the other hand, the existence of oxidised layer could postpone the wear of the specimen by reducing real contact between the counterpart ball and the surface of the coating.[25] The SEM images in Fig. 3 show that the worn surface of the AC-HVAF coating can form a more complete and higher fraction of oxidised tribolayer than that of the HVOF coating under the same test conditions, resulting in the more superior wear resistance of the AC-HVAF coating. Since the higher fraction of oxidised tribolayer plays an important role in enhancing the wear resistance of the AC-HVAF coating, it is necessary to investigate the difference in oxidised tribolayers of the amorphous coatings.

Figure 4*c* and *d* shows the worn-off debris of amorphous coatings prepared by HVOF and AC-HVAF. The debris worn-off from the as-deposited coatings mainly consist of small angular particles and some large flakes. As seen from Fig. 4*c*, small particles (section K) contain similar oxygen content compared with the island region (section G). Although the oxygen content of large flakes (section J) is relatively lower, it is still much higher than that of smooth regions of the wear track (section B). Therefore, these two types of debris are thought to be peeled off from the highly oxidised local regions of the AC-HVAF coating surface. However, for the case of debris worn-off from the HVOF coating, the oxygen content of large flakes (section M) is close to that of smooth regions of the wear track (section D), indicating that this part of debris maybe come from the HVOF coating surface. Meanwhile, the small highly oxidised particles may be generated from local highly oxidised regions or perhaps from large flakes that might be removed and oxidised like the situation happened in the AC-HVAF coating.

Figure 6 shows the SEM images of a longitudinal cross-section of a wear track of the amorphous coatings

Table 2 EDS results (at.-%) of the sections E–M in Fig. 4

Sections	Fe	Cr	Mo	Ni	P	Si	O
E	58.59	8.05	3.90	4.58	12.16	3.16	9.57
F	17.07	2.23	1.20	1.44	3.69	0.97	73.41
G	16.83	2.37	1.21	1.32	3.75	0.94	73.58
H	54.03	7.34	3.69	4.17	11.34	3.06	16.37
I	33.90	4.71	2.17	2.66	6.62	1.52	48.92
J	22.79	3.16	1.28	2.15	4.01	1.03	65.54
K	15.19	2.44	0.94	1.29	3.44	0.93	75.16
L	28.73	3.79	1.83	2.27	5.69	1.35	56.34
M	41.03	5.11	2.44	3.56	8.16	2.06	37.64

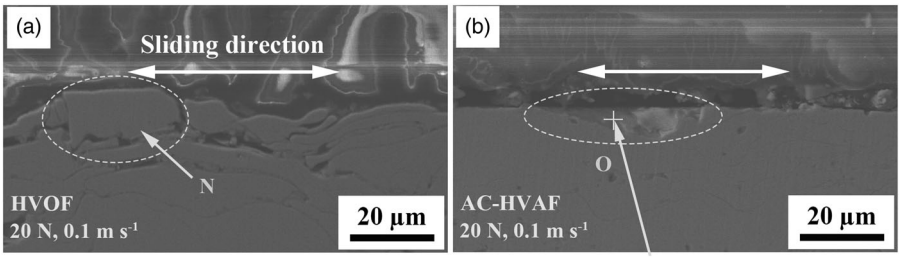

Element	Fe	Cr	Mo	Ni	P	Si	O
At.%	28.10	3.99	1.79	2.17	5.59	1.17	57.19

6 SEM micrographs of a longitudinal cross-section of wear tracks of the amorphous coatings at speed of 0.1 m s^{-1}: *a* the HVOF coating; *b* the AC-HVAF coating

prepared by AC-HVAF and HVOF at speed of 0.1 m s^{-1}. Some micro-cracks are detected on the regions beneath the surface of the HVOF coating. It can be seen that section N in Fig. 6*a* is surrounded by cracks, making it easy to strip from the surface and turn into flake-like debris. Moreover, the length of the section N is around 20 μm, which is very similar to the size of the large flake in Fig. 4*d*. This demonstrates that the large flake-like debris are indeed worn-off from the coating surface. As evidently seen in Fig. 1*d*, there are some heterogeneous phases such as the unmelted particle and intersplat regions in the HVOF coating. Some sprayed powders may form thin oxide layers on the outer sides of their surfaces during in-flight process on account of high temperature and excessive oxygen. When the splats impact to substrate with subsequently flattened and spreading behaviour, the oxide layer on the surface of particle is retained to form a lamellar structure where the interface cohesion is relatively weak.[26,27] Hence, most long-large cracks are found parallel to the coating surface due to the alternating stress in the friction process (Fig. 6*a*). It is regarded that the initiation and propagation of cracks leads to the formation of the large flake-like debris, which would severely damage the oxidised tribolayer formed on the coating surface and also lead to the fluctuation of friction coefficient of the HVOF coating, as shown in Fig. 2. The fluctuation of the friction coefficient is usually attributed to the formation of wear debris and continuous break of the surface tribolayer.[28] However, no obvious micro-cracks can be found in the cross-section of the wear track of the AC-HVAF coating (Fig. 6*b*). The pit in section O has similar oxygen content as compared to that of the wear pit (section I) in the wear tack of the AC-HVAF coating, implying that the selected area is actually located in the wear track of the AC-HVAF coating. Therefore, the AC-HVAF coating has high resistance to initial brittle crack growth. This can be attributed to the dense and fully amorphous microstructure of the AC-HVAF coating, which is good for the formation of a relatively complete and dense oxidised tribolayer.

On the contrary, the worn surfaces of the HVOF coating have much higher roughness than the AC-HVAF coating, as shown in Fig. 3. It has been confirmed that higher surface roughness, that is more contact spaces between the sliding surfaces, could lead to a higher chance of oxidation and higher wear losses.[25,29] Meanwhile, the HVOF coating has more defective regions where the oxygen preferentially diffuses along due to the high atomic activity of these regions, resulting in more serious oxidation on the surface of the HVOF coating. According to the previous discussion, the protective effect of the tribolayer decreases as the oxidation becomes serious, and eventually peels off from the coating surface. Thus, the oxidised tribolayer on the surface of the HVOF coating is easy to damage, leading to the wear resistance of the HVOF coating being inferior to the AC-HVAF coating. In addition, the oxides formed on the surface can reduce adhesive interaction and therefore reduce sliding friction coefficient.[30] The friction coefficient of the HVOF coating should be lower than that of the AC-HVAF coating due to higher surface oxygen content of the former. However, the oxidised tribolayer of the HVOF coating is easy to worn-off resulting in higher surface roughness, which can deteriorate lubricating effect of the oxide tribolayer. Therefore, the friction coefficient of the HVOF coating is only slightly lower than that of the AC-HVAF coating.

Conclusions

The $Fe_{63}Cr_8Mo_{3.5}Ni_5P_{10}B_4C_4Si_{2.5}$ coatings with almost fully amorphous structure have been successfully prepared by AC-HVAF and HVOF techniques. The wear mechanism for the both AC-HVAF and HVOF amorphous coatings is dominated by oxidation wear. However, the AC-HVAF coating shows more superior wear resistance than the HVOF coating during dry sliding conditions. The denser and fully amorphous microstructure achieved by AC-HVAF is beneficial for the formation of a more stable oxidised tribolayer and smoother worn surface, leading to the enhancement of the hardness and wear resistance with the wear volume being approximately seven times less than the HVOF coating. The present results demonstrate that the AC-HVAF technique with less using-cost exhibits the superiority in making Fe-based amorphous coatings for wear applications.

Acknowledgements

This work was supported by National Natural Science Foundation of China (Grant No. 51501210, 51571207 and 51274151) and Ningbo Municipal Nature Science Foundation (Grant No. 2015A610002).

References

1. A. L. Greer, K. L. Rutherford and M. Hutchings: 'Wear resistance of amorphous alloys and related materials', *Int. Mater. Rev.*, 2002, **47**, 87–112.
2. G. Herzer: 'Modern soft magnets: Amorphous and nanocrystalline materials', *Acta Mater.*, 2013, **61**, 718–734.
3. M. J. Duarte, J. Klemm, S. O. Klemm, K. J. J. Mayrhofer, M. Stratmann, S. Borodin, A. H. Romero, M. Madinehei, D. Crespo, J. Serrano, S. S. A. Gerstl, P. P. Choi, D. Raabe and F. U. Renner: 'Element-resolved corrosion analysis of stainless-type glass-forming steels', *Science*, 2013, **341**, 372–376.
4. M. J. Shi, S. J. Pang and T. Zhang: 'Towards improved integrated properties in FeCrPCB bulk metallic glasses by Cr addition', *Intermetallics*, 2015, **61**, 16–20.
5. S. F. Guo, J. L. Qiu, P. Yu, S. H. Xie and W. Chen: 'Fe-based bulk metallic glasses: brittle or ductile?', *Appl. Phys. Lett.*, 2014, **105**, 161901.
6. J. Li, W. Yang, D. Estévez, G. Chen, W. Zhao, Q. Man, Y. Zhao, Z. Zhang and B. Shen: 'Thermal stability, magnetic and mechanical properties of Fe–Dy–B–Nb bulk metallic glasses with high glass-forming ability', *Intermetallics*, 2014, **46**, 85–90.
7. Y. H. Sun: 'Inverse ductile-brittle transition in metallic glasses?', *Mater. Sci. Technol.*, 2015, **31**, 635–650.
8. J. Farmer, J. S. Choi, C. Saw, J. Haslam, D. Day and P. Hailey: 'Iron-based amorphous metals: high-performance corrosion-resistant material development', *Metall. Mater. Trans. A*, 2009, **40**, 1289–1305.
9. Z. B. Zheng, Y. G. Zheng, W. H. Sun and J. Q. Wang: 'Effect of applied potential on passivation and erosion-corrosion of a Fe-based amorphous metallic coating under slurry impingement', *Corros. Sci.*, 2014, **82**, 115–124.
10. W. H. Liu, F. S. Shieu and W. T. Hsiao: 'Enhancement of wear and corrosion resistance of iron-based hard coatings deposited by high-velocity oxygen fuel (HVOF) thermal spraying', *Surf. Coat. Technol.*, 2014, **249**, 24–41.
11. R. Q. Guo, C. Zhang, Q. Chen, Y. Yang, N. Li and L. Liu: 'Study of structure and corrosion resistance of Fe-based amorphous coatings prepared by HVAF and HVOF', *Corros. Sci.*, 2011, **53**, 2351–2356.
12. Y. Wang, Z. Z. Xing, Q. Luo, A. Rahman, J. Jiao, S. J. Qu, Y. G. Zheng, J. Shen: 'Corrosion and erosion–corrosion behaviour of activated combustion high-velocity air fuel sprayed Fe-based amorphous coatings in chloride-containing solutions', *Corros. Sci.*, 2015, **98**, 339–353.
13. S. L. Liu, X. P. Zheng and G. Q. Geng: 'Dry sliding wear behavior and corrosion resistance of NiCrBSi coating deposited by activated combustion-high velocity air fuel spray process', *Mater. Design*, 2010, **31**, 913–917.
14. S. L. Liu, X. P. Zheng and G. Q. Geng: 'Influence of nano-WC-12Co powder addition in WC-10Co-4Cr AC-HVAF sprayed coatings on wear and erosion behaviour', *Wear*, 2010, **269**, 362–367.
15. H. R. Ma, X. Y. Chen, J. W. Li, C. T. Chang, W. Gang, H. Li, X. M. Wang and R. W. Li: 'Synthesis of Fe-based amorphous coating with high corrosion and wear resistance', (Unpublished results).
16. A. Leyland and A. Matthews: 'On the significance of the H/E ratio in wear control: a nanocomposite coating approach to optimised tribological behaviour', *Wear*, 2000, **246**, 1–11.
17. C. Tsotsos, A. L. Yerokhin, A. D. Wilson, A. Leyland and A. Matthews: 'Tribological evaluation of AISI 304 stainless steel duplex treated by plasma electrolytic nitrocarburising and diamond-like carbon coating', *Wear*, 2002, **253**, 986–993.
18. E. Fleury, S. M. Lee, H. S. Ahn, W. T. Kim and D. H. Kim: 'Tribological properties of bulk metallic glasses', *Mater. Sci. Eng. A*, 2004, **375–377**, 276–279.
19. J. Kong, D. S. Xiong, J. L. Ji, Q. X. Yuan and R. Tyagi: 'Effect of flash temperature on tribological properties of bulk metallic glasses', *Tribol. Lett.*, 2009, **35**, 151–158.
20. C. Zhang, L. Liu, K. C. Chan, Q. Chen and C. Y. Tang: 'Wear behavior of HVOF-sprayed Fe-based amorphous coatings', *Intermetallics*, 2012, **29**, 80–85.
21. B. Zhang, W. Wang and G. P. Zhang: 'Depth dependent hardness variation in Ni-P amorphous film under nanoindentation', *Mater. Sci. Technol.*, 2006, **22**, 734–737.
22. K. H. Hou, M. C. Jeng and M. D. Ger: 'A study on the wear resistance characteristics of pulse electroforming Ni-P alloy coatings as plated', *Wear*, 2007, **262**, 833–844.
23. U. Matik and R. Citak: 'Influence of the heat treatment on hardness and adhesive wear performance of Ni-P deposit with low phosphorus content', *Mater. Test.*, 2015, **57**, 431–436.
24. W. Wang, C. Zhang, P. Xu, M. Yasir and L. Liu: 'Enhancement of oxidation and wear resistance of Fe-based amorphous coatings by surface modification of feedstock powders', *Mater. Des.*, 2015, **73**, 35–41.
25. K. T. Cho, Y. K. Lee and W. B. Lee: 'Wear behavior of AISI D2 steel by enhanced ion nitriding with atomic attrition', *Tribol. Int.*, 2015, **87**, 82–90.
26. J. Kim, K. Kang, S. Yoon, S. Kumar, H. Na and C. Lee: 'Oxidation and crystallization mechanisms in plasma-sprayed Cu-based bulk metallic glass coatings', *Acta Mater.*, 2010, **58**, 952–962.
27. Z. Zhou, L. Wang, D. Y. He, F. C. Wang and Y. B. Liu: 'Microstructure and wear resistance of Fe-based amorphous metallic coatings prepared by HVOF thermal spraying', *J. Therm. Spray Technol.*, 2010, **19**, 1287–1293.
28. J. L. Mo and M. H. Zhu: 'Tribological oxidation behaviour of PVD hard coatings', *Tribol. Int.*, 2009, **42**, 1758–1764.
29. K. J. Kubiak, T. W. Liskiewicz and T. G. Mathia: 'Effect of surface roughness parameters on thermally sprayed PEEK coatings', *Tribol. Int.*, 2011, **44**, 1427.
30. Z. Zhou, W. M. Rainforth, Q. Luo, P.Eh. Hovsepian, J. J. Ojeda and M. E. Romero-Gonzalez: 'Wear and friction of TiAlN/VN coatings against Al_2O_3 in air at room and elevated temperatures', *Acta Mater.*, 2010, **58**, 2912–2925.